Visualizing the surface magnetism in antiferromagnetic topological insulator $MnBi_2Te_4$

Paul M. Sass[1], Jinwoong Kim[1], David Vanderbilt[1], Jiaqiang Yan[2], and Weida Wu[1]*.

[1]*Department of Physics and Astronomy, Rutgers University, Piscataway, NJ 08854, USA.*

[2]*Materials Science and Technology Division, Oak Ridge National Laboratory, Oak Ridge, Tennessee 37831, USA.*

*Correspondence to: wdwu@physics.rutgers.edu (WW).

Abstract

$MnBi_2Te_4$ is a promising candidate for an antiferromagnetic (AFM) topological insulator, which might host fascinating quantized anomalous Hall effect or axion insulator states in few-molecular layer form[1–5]. The realization of these quantum phenomena in $MnBi_2Te_4$ hinges on the existence of gapped Dirac surface states arising from the uniaxial A-type AFM order (alternating ferromagnetic layers)[1]. However, recent high-resolution angle-resolved photoemission spectroscopy (ARPES) results reveal gapless surface states, suggesting paramagnetic or non-uniaxial A-type magnetic order[6–9]. Here, we present microscopic evidence of the persistence of uniaxial A-type AFM order to the surface layers of $MnBi_2Te_4$ single crystals using magnetic force microscopy (MFM). Our MFM results reveal termination-dependent magnetic contrast across both surface step edges and AFM domain walls, which can be screened by thin layers of soft magnetism. The robust surface A-type order is further corroborated by the observation of termination-dependent surface spin-flop transitions, which have been theoretically proposed decades ago but never observed in natural AFMs[10,11]. Our results not only provide key ingredients for understanding the electronic properties of the AFM topological insulator $MnBi_2Te_4$, but also open a new paradigm for exploring intrinsic surface metamagnetic transitions in natural antiferromagnets[10–12].

Recent progress in topological quantum materials suggest that antiferromagnets (AFM) may host interesting topological states[13]. For example, it has been proposed that an axion insulator state with topological magnetoelectric response could be realized in an antiferromagentic topological insulator (AFM-TI) phase[14,15], where the Z_2 topological states are protected by a combination of time-reversal symmetry and primitive-lattice translation. The AFM-TI state adiabatically connects to a stack of quantum Hall insulators with alternating Chern numbers[16], thus providing a promising route to realizing the quantum anomalous Hall (QAH) effect in a stoichiometric material. The prior observation of the QAH effect in magnetically doped TI thin films is limited to extremely low temperature because of the inherent disorder[17–21], though the disorder effects can be partially alleviated by material engineering[22–24]. The $MnBi_2Te_4$ (MBT) family was predicted and confirmed to be an AFM-TI that may host QAH and axion-insulator states in thin films with odd and even numbers of septuple layers (SLs) respectively[1–3,25,26]. Recent transport measurements on exfoliated thin flakes provide compelling evidence for these predictions[4,5], suggesting gapped topological surface states. On the other hand, recent high-resolution angle-resolved photoemission spectroscopy (ARPES) studies reveal gapless (or small-gap) surface states below the AFM ordering temperature, suggesting a surface relaxation of the A-type order and/or the formation of nanometer-sized magnetic domains[6–9]. The AFM domain structure of $MnBi_2Te_4$ was revealed by imaging of domain walls using magnetic force microscopy (MFM)[27]. The observed domain size is on the order of 10 μm, excluding the speculated nanometer-size domain scenario[9].

Thus, it is crucial to understand the nature of surface magnetism of $MnBi_2Te_4$ to further narrow down the possible scenarios[6–9]. In this letter, we report the observation of alternating termination-dependent magnetic signals on the surface of $MnBi_2Te_4$ single crystals using cryogenic MFM, which provides direct evidence of the persistence of uniaxial A-type AFM order all the way to the surface. Combined with the recent ARPES observations of gapless surface states, our results suggest a tiny magnetic mass gap (<2.5 meV)[9] as the most likely explanation, indicating a very weak coupling between the topological electronic states and the magnetic order. The robust A-type order is further corroborated by the observation of two surface spin-flop transitions on domains with opposite terminations revealed by the magnetic field dependence of the domain contrast. Although they have been theoretically studied for decades[10,11,28], surface spin-flop transitions have only been observed in synthetic AFMs, not in natural ones[12,29–31]. Our results not

only shed new light on the realization of topological states in AFMs, but also open up exciting explorations of surface metamagnetic transitions in functional AFMs.

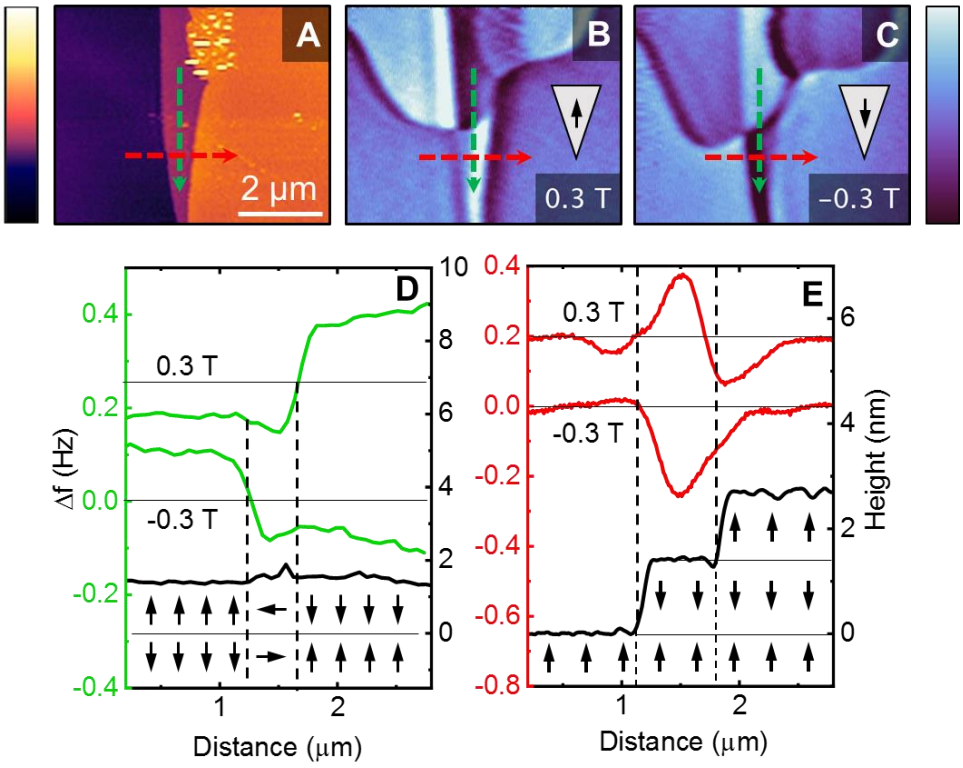

Fig. 1 | Topographic and magnetic force microscopy (MFM) images of as-grown $MnBi_2Te_4$ surface. **A,** Topographic image (5 K) of one and two septuple layer (SL) steps on an as-grown $MnBi_2Te_4$ single crystal. (**B**-**C**) MFM images taken at 0.3 and –0.3 T, respectively, after field cooling at 0.6 T, at the same location as in **A**. A single curvilinear domain was observed cutting through the SL step. Additionally, contrast was observed across SL steps. The domain and SL step contrast was reversed when the tip moment was flipped (dark is attractive and bright is repulsive). **D**-**E**, Line profiles of the topography (black) and MFM (green and red) data. The frequency shift in **D** was measured across the domain wall over flat topography, while in **E** it was taken across the SLs. The color scale for the topographic (MFM) image(s) is 6 nm (0.3 Hz).

For an A-type AFM with ordered moments along the *c*-axis, there are only two possible domain states, up-down-up-down (↑↓↑↓) and down-up-down-up (↓↑↓↑). They are related to each other by either time reversal symmetry or a primitive lattice translation, so they are antiphase

domains and the AFM domains walls separating them are antiphase boundaries. Therefore, there would not be any vertex point connecting three or more domain walls. These expectations are confirmed by our recent cryogenic magnetic force microscopy (MFM) studies in high magnetic fields[27]. The typical domain size is ~10 μm, so the tiny contribution of chiral edge states at domain walls is insufficient to explain the gapless topological surface states[9]. However, it is unclear whether the A-type order persists up to the surface layer, because MFM contrast could come from sub-surface stray fields that penetrate the surface non-magnetic layer[32]. It has been speculated that the observed gapless surface states might be explained by surface relaxation or reorientation of the A-type AFM order[6,8,9]. To address these issues, we carried out MFM studies on as-grown surface of $MnBi_2Te_4$ single crystals with multiple SL steps and thin layers of surface impurity phase. Prior studies suggest that the as-grown surface of $MnBi_2Te_4$ is decorated with small amounts of impurity-phase $Bi_{2-x}Mn_xTe_3$, which is a soft ferromagnet with a small coercive field (<0.04 T)[26,33]. These magnetically soft thin layers provide an excellent opportunity to probe the screening effects of the speculated relaxed surface magnetic order with enhanced magnetic susceptibility[8].

Fig. 1A shows a typical surface morphology of $MnBi_2Te_4$ as-grown surface. There are two step edges in this location, and the observed step height (~1.3 nm) agrees with that of a single SL. Figs. 1B and 1C show the MFM images taken at the same location. Note that one AFM domain wall cuts across the SL steps. Clearly, the magnetic contrast reverses over the domain wall on one terrace (green arrow) and across SLs of one single domain (red arrow) as shown in Fig. 1B and illustrated by line profiles in Fig. 1D and 1E. Here, bright contrast indicates a repulsive interaction, i.e., surface magnetization antiparallel to the MFM tip moment, which is fixed by the external magnetic field. The domain contrast reverses over the domain wall with a slight dip due to the higher susceptibility of the domain wall[27]. This observation is consistent with opposite surface magnetization states of different antiphase domains (Fig. 1D) or SL steps (Fig. 1E). The slight asymmetry in the line profiles in Fig. 1E is due to the difference between forward and backward scanning (see supplementary Fig. S1). The magnetic contrast originates from imperfect cancellation of magnetic stray field from the alternating ferromagnetic layers[34,35]. To confirm this, we reverse MFM tip moment using a negative magnetic field (−0.3 T). The magnetic contrast indeed reverses as shown in Fig. 1C, which unambiguously demonstrates that the alternating MFM signal is from the alternating surface magnetization. Note that there is a small island of impurity phase ($Bi_{2-x}Mn_xTe_3$) with a rougher surface sitting on the upper SL step edge (Fig. 1A). It appears

to screen the AFM domain contrast, as shown in Fig. 1B and 1C. To understand the screening effect of the impurity phase, we increase the scan size to sample more impurity phases.

Fig. 2A shows the topography of a large area with six SL steps in the field of view (~18×13 μm^2). Most steps are paired to form curvy narrow terraces decorated with many plate-like impurity islands with partial hexagon shapes. The height of these island (~3 nm) agrees with that of three quintuple layers (QLs) of Bi_2Te_3, which is slightly larger than that of two SLs (~2.7 nm) as shown in Fig. 2I (see supplementary Fig. S2). Fig. 2B shows the MFM image (measured at 1 T) at this location after 0.425 T field cooling. There are two bubble-like AFM domains with curvilinear domain walls. Alternating magnetic contrast was observed on uncovered SL terraces across step edges or AFM domain walls. However, this contrast is suppressed if the surface is covered by the impurity phases, suggesting a very effective screening of the magnetic stray field. To illustrate the details, zoom-in images of a few selected areas (boxes labelled 1, 2 and 3 in Fig. 2A and 2B) are shown in Fig. 2C-H. Arrows (dashed lines) marked the exposed (covered) narrow terraces in these images. (See supplementary Fig. S3 for a differential map of the topography.) As shown in box 3, the domain contrast can even be "blocked" by a fractional QL of the impurity phase, and clear domain contrast is visible in the holes of the impurity phase. Thus, we can conclude that the magnetic impurity phase ($Bi_{2-x}Mn_xTe_3$) effectively screens all the stray fields from the underlying $MnBi_2Te_4$ surface. Similar results are observed at higher temperature (below T_N). In contrast, AFM domain wall contrast is not affected by the impurity phase as shown in the white dotted box in Fig. 2B, because domain walls extend into the bulk. Because the alternating domain and terrace contrast can be easily screened by such a thin layer (0.3-3 nm) of soft magnet ($Bi_{2-x}Mn_xTe_3$), the uniaxial A-type spin order must persist to the top surface layer of $MnBi_2Te_4$. Otherwise, the termination-dependent magnetic contrast would be screened by any relaxation of surface magnetism with substantial magnetic susceptibility, such as paramagnetism, non-A-type spin order, or in-plane A-type order proposed in prior reports[6–9,36]. Therefore, we can conclude that our MFM observation excludes most of the proposed surface relaxation models, and that the contradictory reports of gapless surface states and a quantized Hall effect remain unresolved.

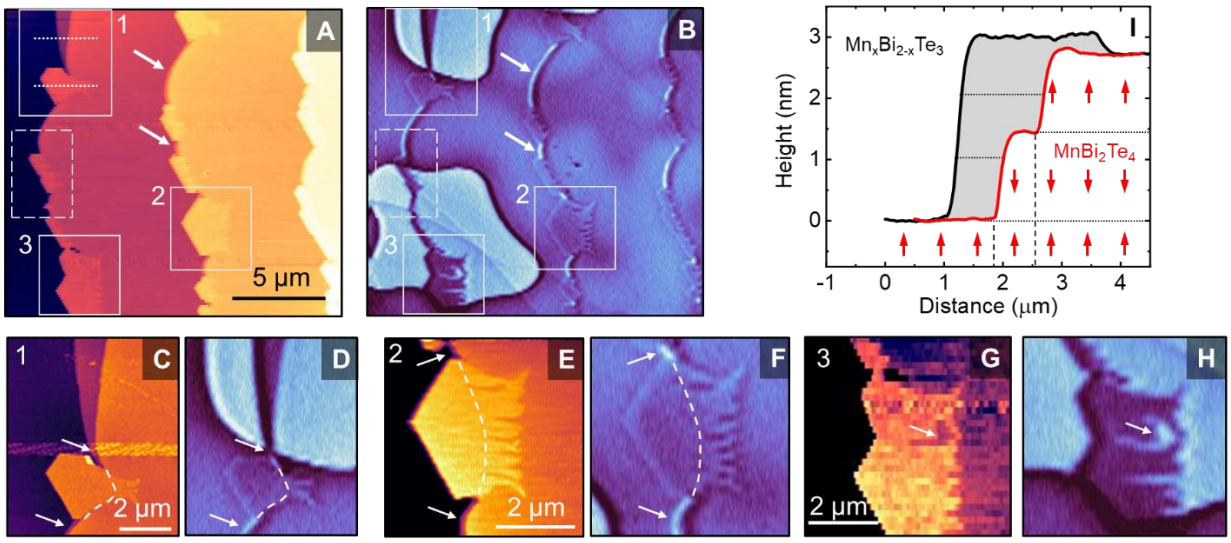

Fig. 2 | Topographic and MFM images on as-grown $MnBi_2Te_4$ illustrating magnetic screening effect of $Bi_{2-x}Mn_xTe_3$ impurity phase. **A**,**B**, Topographic and MFM images of $MnBi_2Te_4$ surface covering a total of seven SLs taken after 0.425 T field cooling and measured in 1 T field at 5 K. Magnetic contrast of domains (~10 μm) and terraces is visible. **C**-**H**, Zoom-ins of topographic and MFM images outlined by solid white boxes in **A**, **B**. White arrows (dashed lines) mark the exposed (covered) single SL steps. The bright domain contrast in box 3 is suppressed by the impurity phase, but spaces appear in the impurity phase that expose the underlying layer and the contrast is no longer suppressed, as shown by white arrow in **H**. Domain wall contrast is not suppressed by the impurity phase, as shown in the dotted box in **B**. **I**, Topographic line profiles (white dotted lines in **A**) of SLs and impurity phase QLs with schematic of spin configuration. The gray area illustrates a soft magnetic phase that screens the stray fields of the SL edges underneath. The color scales for the topographic and MFM images are 7, 6, 3 and 3 nm (0.2 Hz), respectively.

The observation of robust A-type order on the $MnBi_2Te_4$ surface also provides a rare opportunity to explore the interesting "surface spin-flop" (or inhomogeneous spin-flop) transition, which was first proposed by Mills decades ago using an effective one-dimensional spin-chain model with AFM nearest-neighbor exchange coupling[10,11]. However, later studies suggested an intriguing scenario of inhomogeneous spin-flop state due to finite size effect[28,31,37]. The "surface spin-flop" was experimentally observed in synthetic AFMs, which are superlattices of antiferromagnetically coupled ferromagnetic layers[12,30], yet it has not been observed in natural AFMs[28,29]. Because of the existence of domains in natural AFMs, the exploration of surface spin-

flop phenomena requires a surface-sensitive magnetic imaging probe with sufficient spatial resolution in high magnetic field. These challenges were overcome by our cryogenic MFM.

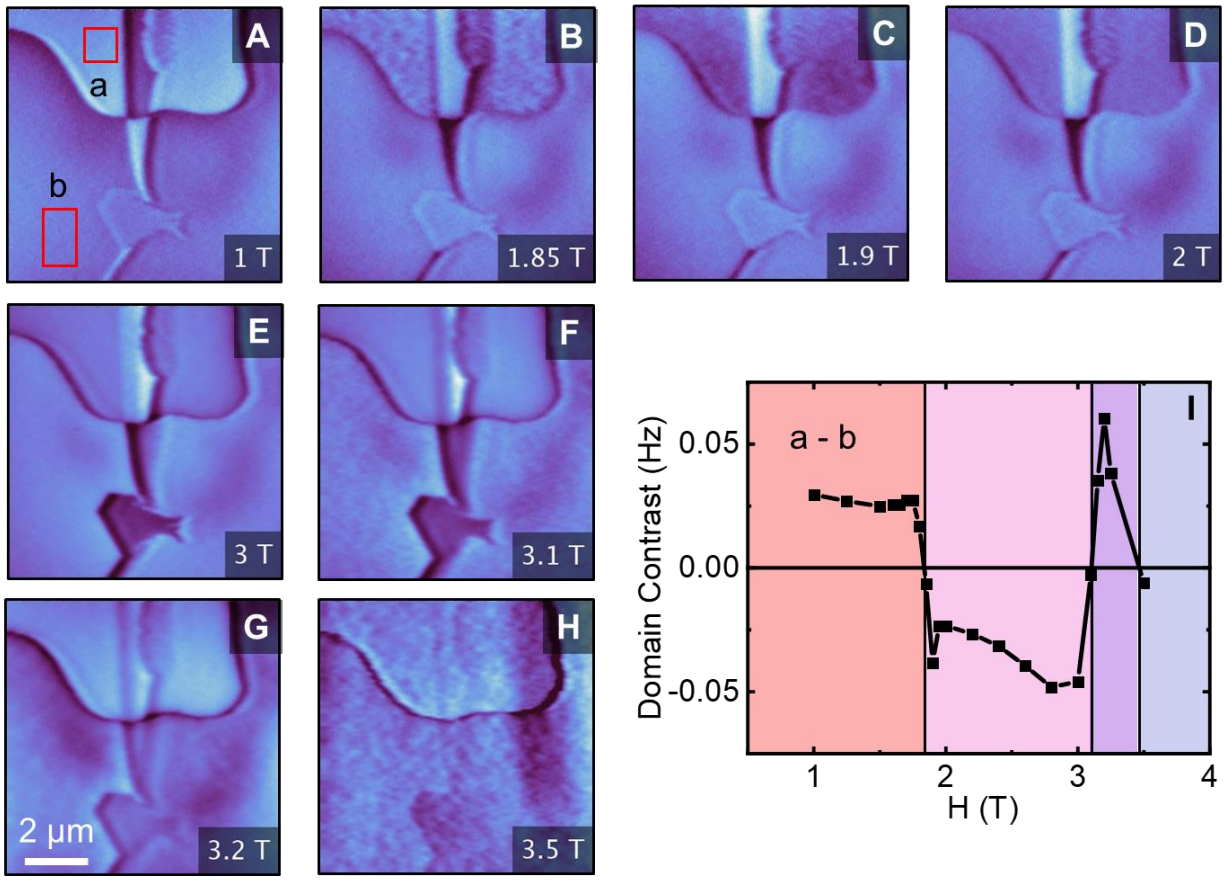

Fig. 3 | MFM images and magnetic field dependence of domain contrast on as-grown $MnBi_2Te_4$. (**A-H**) MFM images taken at 5 K with increasing field labeled in lower right corners. (**I**) Domain contrast between red squares, labeled *a* and *b* in **A** versus applied field. Below 1.75 T, the domain contrast is constant. As the applied field is increased, the domain contrast quickly reverses around 1.85 and 3.1 T. Above 3.5 T, the system enters the canted AFM (CAFM) phase. Near 1.85 T, the bright domain starts to appear rougher and darker, i.e. the antiparallel surface domain undergoes a spin flop. At 3.1 T, the next lower SL flops due to its interaction with the spin-flopped surface layer, and thus, the bright domain again begins to appear rougher and darker. The color scale for MFM images is 0.3 (**A-D**) and 0.8 (**E-H**) Hz.

Figs. 3A-H show selected MFM images measured in various magnetic fields from 1.0 to 3.5 T (see supplementary Fig. S4 for a complete data set). Clearly, the termination-dependent contrast shows non-monotonic magnetic field dependence. As discussed in connection with Fig. 1, in low magnetic field a bright contrast indicates surface termination with antiparallel magnetization (denoted *a* in Fig. 3A), while dark contrast indicates surface termination with

parallel magnetization (denoted *b* in Fig. 3A). This domain contrast persists in finite magnetic field up to ~1.85 T, then fine features start to emerge in termination *a* during the domain contrast reversal, while the termination *b* remains featureless. Thus, it is the termination *a* (antiparallel magnetization) that undergoes surface spin-flop (SSF) transition at H_{SSF}^{1}1.85 T. Similar behavior was observed at ~3.1 T except the roles of *a* and *b* are switched. Thus, it is the termination *b* (parallel magnetization) that undergoes surface spin-flop transition at H_{SSF}^{2}3.1 T. Finally, the domain contrast disappears around the bulk spin-flop (BSF) transition ($H_{\mathrm{BSF}}3.5T$). The detailed field dependence of domain contrast is plotted in Fig. 3I, where the domain contrast is defined as the difference of the average MFM signals in the two regions (domain *a* and *b*) marked by red boxes in Fig. 3A. This effect is also observed in negative applied field and is reproducible in other sample locations after thermal cycling and on a cleaved crystal of $MnBi_2Te_4$ (see supplementary Figs. S5-S7). No hysteresis was found between up-sweep and down-sweep of the magnetic field.

The first SSF transition $\left(H_{\mathrm{SSF}}^{1} \approx 0.5H_{\mathrm{BSF}}\right)$ agrees well with prior observation in synthetic AFMs[12], and is in reasonable agreement with that of the Mills model $\left(H_{\mathrm{SSF}}^{th} \approx 0.7H_{\mathrm{BSF}}\right)$.[11,37] However, the second surface spin-flop transition $\left(H_{\mathrm{SSF}}^{2} \approx 0.9H_{\mathrm{BSF}}\right)$ of the surface with parallel magnetization termination is unexpected in prior studies[28,30,37], indicating surface relaxation of the A-type AFM order. To confirm this, we studied the revised Mills model with additional surface relaxation effects such as reduced magnetization, exchange coupling, and/or anisotropy energy[28]. (See method and supplementary note 5 for details.)

In the original Mills model, the antiparallel surface nucleates a horizontal domain wall with a spin-flop state that migrates into the bulk, forming an inhomogeneous state that precedes the bulk spin-flop transition.[11,28,37] If the migration indeed occurs, the antiparallel surface would sequentially turn into a parallel surface, resulting in an identical magnetization state on the two domains, *i.e.*, no domain contrast above the SFF transition. Such behavior is inconsistent with our experimental observation of domain contrast reversal. Our simulation reveals that the horizontal domain wall with spin-flop state can be pinned to surface layers if the magnetization of surface layer is reduced by more than 10% (see supplementary information note 5). Indeed, the revised Mills model with surface relaxation effect can reproduce the two successive SSF transitions in a reasonably wide parameter space.

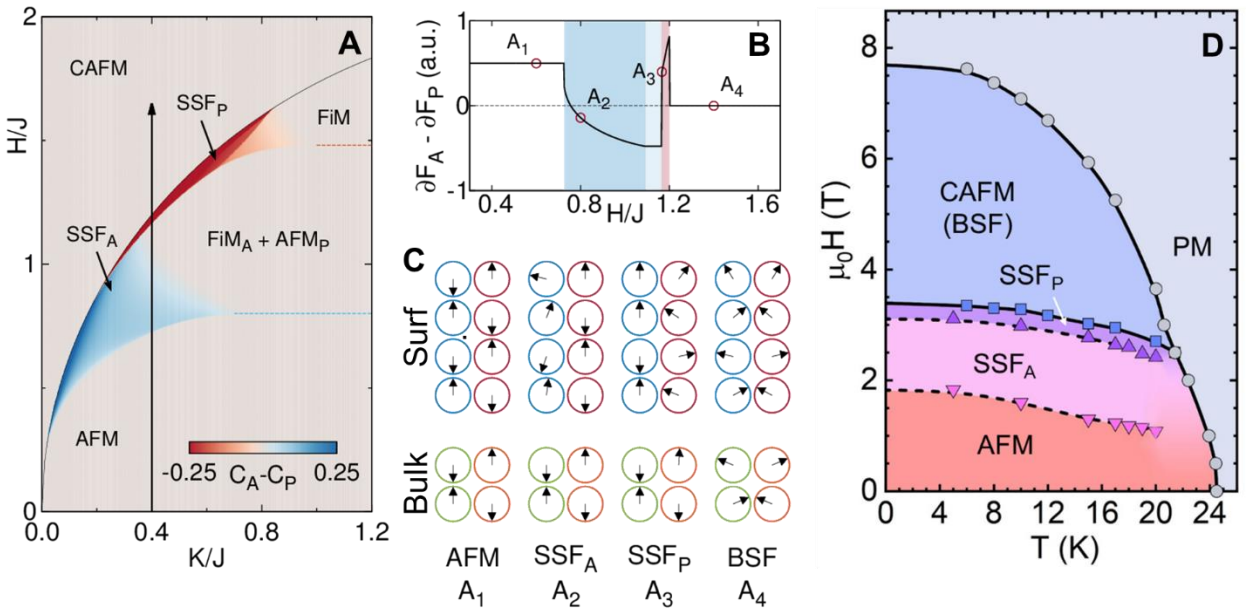

Fig. 4 | Simulated phase diagrams and domain contrast of surface spin-flop process, schematic of spin-structure, and experimental *H-T* phase diagram of $MnBi_2Te_4$. (**A**) Theoretical phase diagram of the spin-flop state in the revised Mills model. Blue and red colored regimes illustrate surface spin-flop states for antiparallel and parallel surfaces, respectively. Color code denotes the difference of net spin canting between the two types of surfaces (see text). Black solid line is a phase boundary of the bulk spin-flop state; dashed line is a boundary between AFM and surface spin-flip phases for antiparallel (blue) and parallel (red) surfaces. (**B**) Simulated magnetic force gradient differences between antiparallel and parallel surfaces with respect to the external field. (**C**) Schematic illustration of the spin-flop process for surface (upper 4 rows) and bulk (lower) domains. Left blue (right red) represents antiparallel (parallel) surface spins, whereas, left green (right yellow) represents antiparallel (parallel) bulk spins. (**D**) *H-T* phase diagram showing A-type AFM phase (red), SSF_A and SSF_P spin-flop phase (pink and light purple), bulk CAFM phase (dark purple), and forced ferromagnetic or paramagnetic (PM) phase (light blue).

Fig. 4A shows a phase diagram of the simulation using typical parameters exhibiting the emergent sequential SSF transitions on antiparallel (blue) and parallel (red) surfaces, respectively. In addition, the reduction of surface exchange coupling could explain the suppression of the SSF transition. The simulated MFM contrast (force gradient difference) as a function of magnetic field is shown in Fig. 4B, qualitatively agreeing with the experimental observation shown in Fig. 3I. (See Methods and supplementary note 5 for details.) The successive SSF and BSF transitions are

summarized schematically in Fig. 4C. The antiparallel surface layer (blue) undergoes a SSF transition H_{SSF}^{1} where the MFM contrast reverses. The domain contrast increases even further in this region, likely due to an increasing canted moment of the spin-flop state. At the next critical field H_{SSF}^{2}, the parallel surface (red) undergoes SSF transition, resulting in another reversal of the MFM contrast. Finally, the MFM domain contrast disappears above the BSF transition because both domains have the same canted moments.

To explore the impact of thermal fluctuations, we performed MFM studies at higher temperatures below T_N to extract the T dependence of the SSF transitions $\left(H_{SSF}^{1} \text{ and } H_{SSF}^{2}\right)$ (see supplementary Fig. S10). As shown in Fig. 4D, the temperature dependence of both SSF transitions follow that of the BSF (H_{BSF}), which gradually reduces with increasing temperature until the bicritical point (~21 K, ~2.5 T), indicating the relative energetics of the SSF transitions do not vary much with temperature. Above 21 K, the AFM domains become unstable in finite magnetic field because of enhanced thermal fluctuations, making it difficult to determine the SSF transitions in this temperature window.

In summary, our MFM results provide microscopic evidence of robust uniaxial A-type order that persists to the top surface layers in the antiferromagnetic topological insulator $MnBi_2Te_4$. Thus, our results strongly constrain the possible mechanisms of the observed gapless topological surface states. Furthermore, we observed, for the first time, the long-sought surface spin-flop transition in natural antiferromagnets. More interestingly, we discovered an additional surface spin-flop transition on the parallel magnetization surface, which indicates surface relaxation of the A-type order. The MFM observation of the surface spin-flop transition not only opens a new paradigm for visualizing surface metamagnetic transitions in antiferromagnetic spintronic devices, but also provides new insights into the realization of the quantum anomalous Hall or axion-insulator states in topological anitferromagnets[4,5].

Methods

Sample preparation. Platelike single crystals of $MnBi_2Te_4$ were grown out of a Bi-Te flux and have been well characterized by measuring the magnetic and transport properties. They order magnetically below T_N = 24 K with ferromagnetic Mn-Te layers coupled antiferromagnetically.

At 2 K, $MnBi_2Te_4$ shows a spin-flop transition at $\mu_0 H_{SF} = 3.5$ T w followed by moment saturation at saturation transition at $\mu_0 H_S = 7.8$ T with a magnetic field applied along the crystallographic *c*-axis.

MFM measurement. The MFM experiments were carried out in a homemade cryogenic magnetic force microscope using commercial piezoresistive cantilevers (spring constant $k \approx 3$ N/m, resonant frequency $f_0 \approx 42$ kHz). The homemade MFM is interfaced with a Nanonis SPM Controller (SPECS) and a commercial phase-lock loop (SPECS). MFM tips were prepared by depositing nominally 150 nm Co film onto bare tips using e-beam evaporation. MFM images were taken in a constant height mode with the scanning plane nominally ~100 nm (except specified) above the sample surface. The MFM signal, the change of cantilever resonant frequency, is proportional to out-of-plane stray field gradient. Electrostatic interaction was minimized by nulling the tip-surface contact potential difference. Dark (bright) regions in MFM images represent attractive (repulsive) magnetization, where magnetizations are parallel (anti-parallel) with the positive external field.

Simulation. The numerical simulations were performed with the revised Mills model,

$$E = \sum_{i=1}^{N-1} J_i s_i \cdot s_{i+1}$$

where $\lambda_A, (A = s, J, K)$ represents the reduction of surface magnetization, exchange coupling, and anisotropy energy, respectively. The reduced surface magnetization causes a pinning of the spin-flop state at the surface (see supplementary information). One end of the system described by a "clamped boundary condition" in which the spin constrained to that of the bulk,

$$\theta_{i=N} = \theta_{Bulk} = \begin{cases} 0, \wedge H_{FM} < H \\ \pm cos^{-1}\dfrac{H}{H_{FM}}, \wedge H_{BSF} < H \leq H_{FM} \\ (\pm 1 - 1)\dfrac{\pi}{2}, \wedge H \leq H_{BSF} \end{cases},$$

where $H_{FM} = 4J - K$ and $H_{BSF} = \sqrt{K(4J - K)}$ are threshold fields for the bulk forced ferromagnetic and bulk spin-flop transitions respectively, the anisotropy $K < 2J$ is assumed to be small, and the sign indicates two types of surfaces: + for parallel and – for antiparallel.

The phase diagram of a semi-infinite system is obtained by using of revised Mills model with the one-side-clamped boundary condition for $N = 16$ layers with a parameter set of ($K/J = 0.4, \lambda_s = 0.6$, $\lambda_J = 0.8$, and $\lambda_K = 0.6$). The ground state at each sampling point is searched by comparing total energies of spin configurations relaxed from 200 initial random configurations. Two SSF states in the phase diagram are illustrated by comparing the net spin canting of two surfaces, which is defined as $C_{A,P} \equiv 1/N \sum_{i=1}^{N} sin^2\left(\theta_i^{A,P}\right)$ for antiparallel (A) and parallel (P) surfaces. The difference $C_A - C_P$ vanishes if both surfaces are in the bulk spin-flop (BSF) state or collinear states, and remains finite only when one surface is in the SSF state. To simulate the MFM contrast, the force gradient is calculated as $\partial F = \sum_{i=1}^{1000} cos(\theta_i)/\left(d + t(i-1)\right)^5$, where $d = 150$ nm is the tip height from the surface, $t = 13.6$ Å is the thickness of one septuple layer, and θ_i is a zenith angle of the *i*-th layer. For $i \geq N$, the angles are constrained or assumed to be that of bulk.

Data availability -- The data that support the findings of this study are available from the corresponding author upon reasonable request.

References

1. Otrokov, M. M. *et al.* Unique Thickness-Dependent Properties of the van der Waals Interlayer Antiferromagnet $MnBi_2Te_4$. *Phys. Rev. Lett.* **122**, 107202 (2019).
2. Gong, Y. *et al.* Experimental realization of an intrinsic magnetic topological insulator. *Chin. Phys. Lett.* **36**, 076801 (2019).
3. Otrokov, M. M. *et al.* Prediction and observation of the first antiferromagnetic topological insulator. *Nature* **576**, 416–422 (2019).
4. Liu, C. *et al.* Robust axion insulator and Chern insulator phases in a two-dimensional antiferromagnetic topological insulator. *Nat. Mater.* (2020). doi:10.1038/s41563-019-0573-3
5. Deng, Y. *et al.* Quantized anomalous Hall effect in intrinsic magnetic topological insulator $MnBi_2Te_4$. *Science (80-.).* **367**, 895–900 (2020).
6. Li, H. *et al.* Dirac surface states in intrinsic magnetic topological insulators EuSn2As2 and MnBi2Te4. *Phys. Rev. X* **9**, 041039 (2019).
7. Swatek, P. *et al.* Gapless Dirac surface states in the antiferromagnetic topological insulator MnBi2Te4. *arXiv:1907.09596* 1–6 (2019).
8. Hao, Y.-J. *et al.* Gapless surface Dirac cone in antiferromagnetic topological insulator

$MnBi_2Te_4$. *Phys. Rev. X* **9**, 041038 (2019).

9. Chen, Y. J. *et al.* Topological Electronic Structure and Its Temperature Evolution in Antiferromagnetic Topological Insulator MnBi2Te4. *Phys. Rev. X* **9**, 041040 (2019).

10. Mills, D. L. Surface spin-flop state in a simple antiferromagnet. *Phys. Rev. Lett.* **20**, 18–21 (1968).

11. Keffer, F. & Chow, H. Dynamics of the antiferromagnetic spin-flop transition. *Phys. Rev. Lett.* **31**, 1061–1063 (1973).

12. Böhm, B. *et al.* Antiferromagnetic domain wall control via surface spin flop in fully tunable synthetic antiferromagnets with perpendicular magnetic anisotropy. *Phys. Rev. B* **100**, 140411 (2019).

13. Šmejkal, L., Mokrousov, Y., Yan, B. & Macdonald, A. H. Topological antiferromagnetic spintronics. *Nat Phys* **14**, 242–251 (2018).

14. Mong, R. S. K., Essin, A. M. & Moore, J. E. Antiferromagnetic topological insulators. *Phys. Rev. B* **81**, 245209 (2010).

15. Varnava, N. & Vanderbilt, D. Surfaces of axion insulators. *Phys Rev B* **98**, 245117 (2018).

16. Haldane, F. D. Model for a quantum Hall effect without Landau levels: Condensed-matter realization of the 'parity anomaly'. *Phys Rev Lett* **61**, 2015–2018 (1988).

17. Chang, C.-Z. *et al.* Experimental Observation of the Quantum Anomalous Hall Effect in a Magnetic Topological Insulator. *Science (80-.).* **340**, 167–170 (2013).

18. Chang, C. Z. *et al.* Zero-Field Dissipationless Chiral Edge Transport and the Nature of Dissipation in the Quantum Anomalous Hall State. *Phys Rev Lett* **115**, 057206 (2015).

19. Kou, X. *et al.* Metal-to-insulator switching in quantum anomalous Hall states. *Nat Commun* **6**, 8474 (2015).

20. Checkelsky, J. G. *et al.* Trajectory of the anomalous Hall effect towards the quantized state in a ferromagnetic topological insulator. *Nat Phys* **10**, 731–736 (2014).

21. Lachman, E. O. *et al.* Visualization of superparamagnetic dynamics in magnetic topological insulators. *Sci. Adv.* **1**, 1500740 (2015).

22. Mogi, M. *et al.* Magnetic modulation doping in topological insulators toward higher-temperature quantum anomalous Hall effect. *Appl. Phys. Lett.* **107**, 182401 (2015).

23. Ou, Y. *et al.* Enhancing the quantum anomalous Hall effect by magnetic codoping in a topological insulator. *Adv Mater* **30**, 1703062 (2017).

24. Wang, W. *et al.* Direct evidence of ferromagnetism in a quantum anomalous Hall system. *Nat. Phys.* **14**, 791–795 (2018).

25. Yan, J. Q.-Q. *et al.* Evolution of structural, magnetic and transport properties in $MnBi_{2-x}Sb_xTe_4$. *Phys. Rev. B* **100**, 104409 (2019).

26. Yan, J.-Q. *et al.* Crystal growth and magnetic structure of $MnBi_2Te_4$. *Phys. Rev. Mater.* **3**, 064202 (2019).

27. Sass, P. M. *et al.* Magnetic imaging of domain walls in the antiferromagnetic topological insulator $MnBi_2Te_4$. *Nano Lett.* **Online pub**, (2020).

28. Rößler, U. K. & Bogdanov, A. N. Reorientation in antiferromagnetic multilayers: Spin-flop transition and surface effects. *Phys. Status Solidi C Conf.* **1**, 3297–3305 (2004).

29. Wang, R. W. & Mills, D. L. Magnetic properties of finite antiferromagnetic superlattices: Statics, dynamics, and the surface spin-flop phase. *Phys. Rev. B* **50**, 3931–3941 (1994).

30. Wang, R. W., Mills, D. L., Fullerton, E. E., Mattson, J. E. & Bader, S. D. Surface spin-flop transition in Fe/Cr(211) superlattices: Experiment and theory. *Phys. Rev. Lett.* **72**, 920–923 (1994).

31. Pini, M. G. *et al.* Surface spin-flop transition in a uniaxial antiferromagnetic Fe/Cr superlattice induced by a magnetic field of arbitrary direction. *J. Phys. cond. mater.* **19**, 136001 (2007).

32. Geng, Y., Lee, N., Choi, Y. J., Cheong, S. W. & Wu, W. Collective magnetism at multiferroic vortex domain walls. *Nano Lett.* **12**, 6055–6059 (2012).

33. Hor, Y. S. *et al.* Development of ferromagnetism in the doped topological insulator $Bi_{2-x}Mn_xTe_3$. *Phys. Rev. B* **81**, 195203 (2010).

34. Hamada, S., Himi, K., Okuno, T. & Takanashi, K. MFM observation of perpendicular magnetization and antiferromagnetically coupled domains in Co/Ru superlattices. *J. Magn. Magn. Mater.* **240**, 539–542 (2002).

35. Hellwig, O., Berger, A. & Fullerton, E. E. Domain Walls in Antiferromagnetically Coupled Multilayer Films. *Phys. Rev. Lett.* **91**, 197203 (2003).

36. Ma, X. *et al.* Hybridization-Induced Gapped and Gapless States on the Surfaces of Magnetic Topological Insulators. *arXiv:1912.13237* (2019).

37. Morosov, A. I. & Sigov, A. S. Surface spin-flop transition in an antiferromagnet. *Physics-Uspekhi* **53**, 677–689 (2010).

Acknowledgement

The MFM studies at Rutgers is supported by the Office of Basic Energy Sciences, Division of Materials Sciences and Engineering, US Department of Energy under Award numbers DESC0018153. The simulation efforts is supported by ONR Grants N00014-16-1-2951. Work at ORNL was supported by the US Department of Energy, Office of Science, Basic Energy Sciences, Materials Sciences and Engineering Division.

Author Contributions

W.W. conceived and supervised the project. J.Y. synthesized the MBT single crystals. P.S. performed the MFM and in-situ transport experiments and analyzed the data. J.K. and D.V. performed the model simulation. P.S., J.K. and W.W. wrote the manuscript with inputs from other authors. All authors discussed the data and contributed to the manuscript.

Competing Interests

The authors declare no competing interests.